

Deuteron photodisintegration within the Quark-Gluon Strings Model and QCD motivated nonlinear Regge trajectories¹

V.Yu. Grishina^a, L.A. Kondratyuk^b, W. Cassing^c, A.B. Kaidalov^b, E. De Sanctis^d and P. Rossi^d

^a*Institute for Nuclear Research, 60th October Anniversary Prospect 7A, 117312 Moscow, Russia*

^b*Institute for Theoretical and Experimental Physics, B. Cheremushkinskaya 25, 117259 Moscow, Russia*

^c*Institute for Theoretical Physics, University of Giessen, Heinrich-Buff-Ring 16, D-35392 Giessen, Germany*

^d*Frascati National Laboratories, INFN, CP 13, via E. Fermi, 40; I-00044, Frascati, Italy*

Abstract

We investigate deuteron two-body photodisintegration within the framework of the Quark-Gluon Strings Model with nonlinear baryon Regge trajectories. Special attention is paid to the use of QCD motivated Regge trajectories of the logarithmic and square-root form which have been suggested recently by Brisudová, Burakovsky and Goldman. We find that the recent experimental data from TJNAF in the few GeV region can reasonably be described by the model. Angular distributions at different γ -energies are presented and the effect of a forward-backward asymmetry is discussed. Predictions for the energy dependence of $d\sigma/dt$ at higher energies and different Θ_{cm} are presented, too.

PACS: 12.40.Nn; 12.40.Vv; 13.40.-f; 25.20.-x

Keywords: Regge theory, duality; Vector-meson dominance; Electromagnetic processes and properties; Photonuclear reactions

¹Supported by DFG and RFFI.

1 Introduction

Recent experiments on high energy two-body photodisintegration of the deuteron [1]-[3] have brought up interesting results: while the 89° and 69° data are consistent with the constituent-quark counting-rule behavior [4] (i.e. at fixed c.m. angle the differential cross section $d\sigma/dt_{\gamma d \rightarrow pn}$ scales as $\sim s^{-11}$), the 36° and 52° data do not show a scaling behavior at all up to 4.0 GeV photon energy. Thus perturbative QCD (PQCD) cannot be applied at these energies at forward angles and nonperturbative approaches have to be used instead.

Some time ago a nonperturbative approach based on the Quark-Gluon Strings Model (QGSM) has been applied to the analysis of the angular and energy dependence of the differential cross section for the $\gamma d \rightarrow pn$ reaction in the few GeV energy region [5]. In the QGSM – proposed in Ref. [6] for the description of binary hadronic reactions – the amplitude of the reaction $\gamma d \rightarrow pn$ is described by the exchange of three valence quarks in the t -channel with any number of gluon exchanges between them. This process is visualized in Fig. 1, where a) and b) describe the exchange of three valence quarks in the t - and u -channels, respectively.

We recall that the QGSM is based on two ingredients: i) a topological expansion in QCD and ii) the space-time picture of the interactions between hadrons, that takes into account the confinement of quarks. The $1/N$ expansion in QCD (where N is the number of colors N_c or flavors N_f) was proposed by 't Hooft [7]; the behavior of different quark-gluon graphs according to their topology, furthermore, was analyzed by Veneziano [8] with the result that in the large N limit the planar quark-gluon graphs become dominant. This approach based on the $1/N_f$ expansion [8] with $N_c \sim N_f$ was used by Kaidalov [6, 9] in the formulation of the QGSM. Again for sufficiently large N_f the simplest planar quark-gluon graphs give the dominant contribution to the amplitudes of binary hadronic reactions. Moreover, it can be shown that in the space-time representation the dynamics described by planar graphs corresponds to the formation and break-up of a quark-gluon string (or color tube) in various intermediate states (see e.g. Refs. [10, 11, 12, 13, 14]). Here the quark-gluon string can be identified with a corresponding Regge trajectory². In this sense the QGSM can be considered as a microscopic model of Regge phenomenology and be used for the calculation of different parameters, that have been considered before only on a phenomenological level.

As shown in Refs. [6, 9] the QGSM describes rather well the experimental data on exclusive and inclusive hadronic reactions at high energy. Moreover, due to the duality property of scattering amplitudes this approach can also be applied at intermediate energies for reactions without explicit resonances in the direct channel. In fact, this model successfully describes the reactions $pp \rightarrow d\pi^+$, $\bar{p}d \rightarrow MN$ and $\gamma d \rightarrow pn$ at intermediate energies, too, where the diagrams with three valence quark exchanges in the t -channel were found to be dominant (cf. Refs. [5, 15, 16]). However, in all those cases the explicit spin structure of the corresponding amplitudes was not taken into account. On the other hand, spin effects and the transversal polarization of the photon lead to a nontrivial an-

²In case of Fig.1 we have in the intermediate state a string with a quark and a diquark at the ends which corresponds to a nucleon Regge trajectory

gular dependence of the residue of the amplitude for the reaction $\gamma d \rightarrow pn$ as discussed in Ref. [5]. In this paper we will use an extended approach to the spin effects in the QGSM as developed in Ref. [17] with respect to the description of the electromagnetic nucleon form factors F_1 and F_2 .

Another important extension of the QGSM in our study will be the use of nonlinear baryon Regge trajectories. There are phenomenological evidences (see [18, 19, 20]) as well as theoretical arguments (see e.g. [21] and references therein) that hadronic Regge trajectories should be nonlinear. This nonlinearity is not important for small momentum transfer (squared) t , however, in the region of t , which has already been reached in the experiment [1], effects of nonlinearity become very essential. We will employ three different forms of nonlinear nucleon Regge trajectories: i) a phenomenological one, which becomes linear at large t , and two QCD motivated trajectories of ii) logarithmic and iii) square-root type as suggested recently by Brisudová, Burakovsky and Goldman [21]. By extrapolating our amplitudes to large angles we can figure out to what momentum transfer t the 'soft QGSM tails' are still important before the PQCD regime becomes dominant.

In Section 2 we outline the QGSM and its relation to Regge theory and introduce hadron-quark and quark-hadron transition amplitudes that are described by planar graphs. In Section 3 we construct the $\gamma d \rightarrow pn$ amplitude taking into account explicit spin variables. In Section 4 we present the results of our calculations in comparison to the data [1] while Section 5 concludes our present study.

2 The Quark-Gluon Strings Model

In order to introduce the basic features of the QGSM we consider the binary reactions $\pi^0\pi^0 \rightarrow \pi^+\pi^-$, $N\bar{N} \rightarrow \pi^+\pi^-$ and $p\bar{p} \rightarrow N\bar{N}$, which at large values of the invariant energy (squared) s and finite values of the 4-momentum transfer (squared) t can be described by planar diagrams with t -channel valence-quark exchanges as shown by the diagrams a)-c) in Fig. 2. Here the single and double solid lines correspond to valence quarks and diquarks, respectively, while soft gluon exchanges between these lines are not shown. According to the topological $1/N_f$ expansion [8, 9, 22], these planar diagrams are expected to give the dominant contributions to the corresponding amplitudes in the limit $N_f \gg 1$ and $N_c/N_f \sim 1$. In the case of pion and nucleon interactions – as considered here – the exchanges of light u , d , and s quarks are mainly important and the parameter of the expansion is not small, i.e. $1/N_f = 1/3$. However, in case of amplitudes for exclusive reactions with specific quantum numbers in the t -channel, the actual expansion parameter is $1/N_f^2 \sim 1/9$ such that the expansion is expected to work.

2.1 Transition probabilities

Each planar diagram of the topological expansion has a simple interpretation within the framework of the space-time pattern formulated in terms of a color tube (or color string) [9, 23]. As an example we consider the space-time picture of the binary reaction

$\pi^0\pi^0 \rightarrow \pi^+\pi^-$ (cf. Fig.2 a)). At high center-of-mass (c.m.) energy \sqrt{s} , this reaction occurs due to a specific quark configuration in each pion, where (in the c.m. system) one quark (antiquark) takes almost the entire hadron momentum and plays the role of a spectator, while the valence antiquark (quark) is rather slow. The difference in the rapidities Δy between the quark q and antiquark \bar{q} in each pion is

$$\Delta y = y_q - y_{\bar{q}} \simeq \frac{1}{2} \ln \left(\frac{s}{s_0} \right), \quad (1)$$

with the scale $s_0 \simeq 1 \text{ GeV}^2$. Then the two 'slow' valence partons q and \bar{q} from π^0 and π^0 annihilate, and the fast spectator quark and antiquark continue to move in the previous directions and form a color string in the intermediate state. After that, the string breaks due to the production of a $q\bar{q}$ -pair from the vacuum and formation of the $\pi^+\pi^-$ system in the final state. We note, that the same space-time pattern holds for the diagram of Fig. 2 b) with the only difference, that the string is formed after annihilation of a diquark-antidiquark pair from the $N\bar{N}$ -system in the initial state. Correspondingly, the graph of Fig. 2 c) shows the formation of the $q\bar{q}$ string due to annihilation of the valence diquark-antidiquark pair in the initial state and the production of another diquark-antidiquark pair due to the breaking of the string.

The annihilation of the initial $q\bar{q}$ (or $(qq)(\bar{q}\bar{q})$) pair takes place, when the gap in rapidity of the valence q and \bar{q} (or $(qq)(\bar{q}\bar{q})$) is small (both interacting partons are almost at rest in c.m.s.) and the relative impact parameter $|\mathbf{b}_\perp - \mathbf{b}_{0\perp}|$ is less than their interaction radius. It is possible to prove that the probability to find a valence quark with a rapidity y_q at impact parameter \mathbf{b}_\perp inside a hadron can be written as [6, 9, 23]

$$w(y_q - y_0, \mathbf{b}_\perp - \mathbf{b}_{0\perp}) = \frac{c}{4\pi R^2(s)} \exp \left[-\beta(y_q - y_0) - \frac{(\mathbf{b}_\perp - \mathbf{b}_{0\perp})^2}{4R^2(s)} \right], \quad (2)$$

where c is a normalization constant, y_0 is the average rapidity, $\mathbf{b}_{0\perp}$ is the transverse coordinate of the c.m. system in the impact-parameter representation. Furthermore, it is possible to relate the parameter β and the effective interaction radius squared $R^2(s)$ in (2), that specify the quark distribution inside a hadron, to the phenomenological parameters of a Regge trajectory $\alpha_i(t)$ which gives the dominant contribution to the amplitude for the considered planar graph. In this case one gets

$$R^2(s) = R_0^2 + \alpha'_i(y_q - y_0), \quad \beta = 1 - \alpha_i(0), \quad (3)$$

where $\alpha'_i = \alpha'_i(0)$ is the slope of the dominant Regge trajectory.

Due to the creation of a string in the intermediate state the amplitude of a binary reaction $ab \rightarrow cd$ has the s -channel factorization property, i.e. the probability for the string to produce different hadrons in the final state does not depend on the type of the annihilated quarks and is only determined by the flavours of the produced quarks. The same independence also holds for the production of the color string in the intermediate state from the initial hadron configuration: it depends only on the type of the annihilated quarks. This s -channel factorization has been formulated in Refs. [6], [9], [23] in terms of transition probabilities as defined by Eq. (2).

2.2 Transition amplitudes

Following Ref. [17] we now generalize this approach by introducing the amplitudes $\tilde{T}^{ab \rightarrow q\bar{q}}(s, \mathbf{b}_\perp)$ and $\tilde{T}^{q\bar{q} \rightarrow cd}(s, \mathbf{b}_\perp)$, that describe the formation and the fission of an intermediate string, respectively. The amplitude for the binary reaction $ab \rightarrow cd$ described by the planar graph of Fig.1a) (b) or c)) can be written – employing the s -channel factorization property – as a convolution of two amplitudes, i.e.

$$A^{ab \rightarrow cd}(s, \mathbf{q}_\perp) = \frac{i}{8\pi^2 s} \int d^2 \mathbf{k}_\perp T^{ab \rightarrow q\bar{q}}(s, \mathbf{k}_\perp) T^{q\bar{q} \rightarrow cd}(s, \mathbf{q}_\perp - \mathbf{k}_\perp) \quad (4)$$

in momentum representation, or as the product

$$\tilde{A}^{ab \rightarrow cd}(s, \mathbf{b}_\perp) = \frac{i}{2s} \tilde{T}^{ab \rightarrow q\bar{q}}(s, \mathbf{b}_\perp) \tilde{T}^{q\bar{q} \rightarrow cd}(s, \mathbf{b}_\perp) \quad (5)$$

in impact-parameter representation.

The solution for the quark-hadron transition amplitudes $T^{q\bar{q} \rightarrow \pi\bar{\pi}}(s, \mathbf{k}_\perp)$ and $T^{q\bar{q} \rightarrow N\bar{N}}(s, \mathbf{k}_\perp)$ at large invariant energy \sqrt{s} can be found using single Regge-pole parameterizations of the binary hadronic amplitudes $A^{\pi^0 \pi^0 \rightarrow \pi^+ \pi^-}$, $A^{N\bar{N} \rightarrow \pi\bar{\pi}}$ and $A^{N\bar{N} \rightarrow N\bar{N}}$

$$\begin{aligned} A^{\pi^0 \pi^0 \rightarrow \pi^+ \pi^-}(s, t) &= N_M \left(-\frac{s}{m_0^2} \right)^{\alpha_M(t)} \exp(R_{0M}^2 t), \\ A^{N\bar{N} \rightarrow \pi\bar{\pi}}(s, t) &= N_B \left(-\frac{s}{m_0^2} \right)^{\alpha_B(t)} \exp(R_{0B}^2 t), \\ A^{N\bar{N} \rightarrow N\bar{N}}(s, t) &= N_D \left(-\frac{s}{m_0^2} \right)^{\alpha_D(t)} \exp(R_{0D}^2 t). \end{aligned} \quad (6)$$

Here $\alpha_M(t)$, $\alpha_B(t)$ and $\alpha_D(t)$ are the dominant meson, baryon and diquark-antidiquark trajectories while N_M , N_B and N_D are normalization constants; $m_0^2 = s_0$ and R_{0i} is the interaction radius for the i -th trajectory. We have the following intercepts and slopes for the dominant Regge trajectories

$$\alpha_M(0) \simeq 0.5, \quad \alpha_B(0) \simeq -0.5, \quad \alpha_D(0) \simeq -1.5 \quad (7)$$

and

$$\alpha'_M(0) \simeq \alpha'_B(0) \simeq \alpha'_D(0) \simeq 1.0 \text{ GeV}^{-2}. \quad (8)$$

Using equations (5) and (6) we can write the amplitudes $\tilde{T}^{q\bar{q} \rightarrow \pi\bar{\pi}}(s, \mathbf{b}_\perp)$ and $\tilde{T}^{q\bar{q} \rightarrow N\bar{N}}(s, \mathbf{b}_\perp)$ as

$$\begin{aligned} \tilde{T}^{q\bar{q} \rightarrow \pi\bar{\pi}}(s, \mathbf{b}_\perp) &= N_M^{1/2} \frac{1}{2\sqrt{\pi} R_M(s)} \left(-\frac{s}{m_0^2} \right)^{(\alpha_M(0)+1)/2} \exp\left(-\frac{\mathbf{b}_\perp^2}{8R_M^2(s)} \right), \\ \tilde{T}^{q\bar{q} \rightarrow N\bar{N}}(s, \mathbf{b}_\perp) &= N_D^{1/2} \frac{1}{2\sqrt{\pi} R_D(s)} \left(-\frac{s}{m_0^2} \right)^{(\alpha_D(0)+1)/2} \exp\left(-\frac{\mathbf{b}_\perp^2}{8R_D^2(s)} \right), \end{aligned} \quad (9)$$

where $R_M(s)$ and $R_D(s)$ are the effective interaction radii given by

$$R_M^2(s) = R_{0M}^2 + \alpha'_M(0) \ln\left(-\frac{s}{m_0^2}\right),$$

$$R_D^2(s) = R_{0D}^2 + \alpha'_D(0) \ln\left(-\frac{s}{m_0^2}\right).$$
(10)

Now substituting the amplitudes (9) into the factorization formula (5) we get:

$$\tilde{A}^{N\bar{N} \rightarrow \pi\bar{\pi}}(s, \mathbf{b}_\perp) =$$

$$(N_M N_D)^{1/2} \frac{1}{4\pi R_D(s) R_M(s)} \left(-\frac{s}{m_0^2}\right)^{\frac{1}{2}(\alpha_D(0) + \alpha_M(0))} \exp\left[-\mathbf{b}_\perp^2 \left(\frac{1}{8R_M^2(s)} + \frac{1}{8R_D^2(s)}\right)\right].$$
(11)

For consistency of eqs. (11) and (6) we have to require the following relations between the Regge parameters and normalization constants ([6, 9, 22]):

$$2\frac{1}{R_B^2(s)} = \frac{1}{R_M^2(s)} + \frac{1}{R_D^2(s)},$$
(12)

$$2\alpha(0)_B = \alpha_D(0) + \alpha_M(0),$$

$$(N_M N_D)^{1/2} \frac{1}{R_D(s) R_M(s)} = N_B \frac{1}{R_B^2(s)}.$$
(13)

If only light u, d quarks are involved we can assume that ([6, 9, 22])

$$\alpha'_M(0) = \alpha'_B(0) = \alpha'_D(0) \equiv \alpha'(0),$$

$$R_{0M}^2(0) = R_{0B}^2(0) = R_{0D}^2(0) \equiv R_0^2(0),$$
(14)

$$(N_M N_D)^{1/2} = N_B.$$

Then the relations (12) and (13) can be fulfilled at all s . Otherwise, they can only be satisfied at sufficiently large s (cf. Ref. ([22])).

3 Deuteron photodisintegration in the QGSM

Before going over to the case of particles with spin we first present the amplitudes for spinless constituents.

3.1 Spinless particles

Using the same approach as in previous Section we now consider the reaction

$$\gamma d \rightarrow pn. \quad (15)$$

By analogy to Eq. (5) the amplitude corresponding to each quark diagram of Fig. 1 can be written as

$$\tilde{A}^{\gamma d \rightarrow pn}(s, \mathbf{b}_\perp) = \frac{i}{2s} \tilde{T}^{\gamma d \rightarrow q(5q)}(s, \mathbf{b}_\perp) \tilde{T}^{q(5q) \rightarrow pn}(s, \mathbf{b}_\perp), \quad (16)$$

where the amplitudes $\tilde{T}^{\gamma d \rightarrow q(5q)}(s, \mathbf{b}_\perp)$ and $\tilde{T}^{q(5q) \rightarrow pn}(s, \mathbf{b}_\perp)$ are given by (cf. (9))

$$\begin{aligned} \tilde{T}^{\gamma d \rightarrow q(5q)}(s, \mathbf{b}_\perp) &= N_{M(6q)}^{1/2} \frac{1}{2\sqrt{\pi}R_{M(6q)}(s)} \left(-\frac{s}{m_0^2}\right)^{(\alpha_M(0)+1)/2} \exp\left(-\frac{\mathbf{b}_\perp^2}{8R_{M(6q)}^2(s)}\right), \\ \tilde{T}^{q(5q) \rightarrow pn}(s, \mathbf{b}_\perp) &= N_{D(6q)}^{1/2} \frac{1}{2\sqrt{\pi}R_{D(6q)}(s)} \left(-\frac{s}{m_0^2}\right)^{(\alpha_D(0)+1)/2} \exp\left(-\frac{\mathbf{b}_\perp^2}{8R_{D(6q)}^2(s)}\right). \end{aligned} \quad (17)$$

Here the effective interaction radii $R_{M(6q)}(s)$ and $R_{D(6q)}(s)$ are defined as

$$\begin{aligned} R_{M(6q)}^2(s) &= R_{0M(6q)}^2 + \alpha'_M(0) \ln\left(-\frac{s}{m_0^2}\right), \\ R_{D(6q)}^2(s) &= R_{0D(6q)}^2 + \alpha'_D(0) \ln\left(-\frac{s}{m_0^2}\right), \end{aligned} \quad (18)$$

where $R_{0M(6q)}^2$ and $R_{0D(6q)}^2$ are, in general, different from R_{0M}^2 and R_{0D}^2 in Eq. (10).

3.2 Full amplitudes with spin variables

In case of constituents with explicit spin we write the deuteron photodisintegration amplitude in the form

$$\begin{aligned} \langle p_3, \lambda_p; p_4, \lambda_n | \hat{T}(s, \mathbf{p}_{3\perp}) | p_2, \lambda_d; p_1, \lambda_\gamma \rangle = \\ \frac{i}{8\pi^2 s} \int d^2\mathbf{k}_\perp \langle \lambda_p; \lambda_n | \hat{T}^{q(5q) \rightarrow pn}(s, \mathbf{k}_\perp) | \lambda_q; \lambda_{(5q)} \rangle \\ \langle \lambda_q; \lambda_{(5q)} | \hat{T}^{\gamma d \rightarrow q(5q)}(s, \mathbf{p}_{3\perp} - \mathbf{k}_\perp) | \lambda_d; \lambda_\gamma \rangle, \end{aligned} \quad (19)$$

where p_1, p_2, p_3 , and p_4 are the 4-momenta of the photon, deuteron, proton, and neutron, respectively, while λ_i is the s channel helicity of the i -th particle. Furthermore, we make simplifying assumption that the spin of the $(5q)$ state is $1/2$. Then we can write the amplitude $\hat{T}^{\gamma d \rightarrow q(5q)}$ as

$$\begin{aligned} \langle \lambda_q; \lambda_{(5q)} | \hat{T}(s, \mathbf{k}_\perp) | \lambda_d; \lambda_\gamma \rangle = \\ \bar{u}_{\lambda_q}(p_q) \hat{\epsilon}_{\lambda_\gamma} \left(\frac{-\hat{k} + m_q}{k^2 - m_q^2}\right) \hat{\epsilon}_{\lambda_d} v_{\lambda_{(5q)}}(p_{(5q)}) D^{\gamma d \rightarrow q(5q)}(s, \mathbf{k}_\perp), \end{aligned} \quad (20)$$

where ϵ_{λ_d} and $\epsilon_{\lambda_\gamma}$ are the deuteron and photon polarization vectors, $D^{\gamma d \rightarrow q(5q)}(s, \mathbf{k}_\perp)$ is the scalar amplitude and m_q is the quark mass. In analogy to $q\bar{q} \rightarrow N\bar{N}$, which was analysed in Ref. [17], we can describe the spin structure of the amplitude $\hat{T}^{q(5q) \rightarrow pn}$ in terms of eight invariant amplitudes

$$\begin{aligned} \langle \lambda_p; \lambda_n | \hat{T}^{q(5q) \rightarrow pn}(s, \mathbf{k}_\perp) | \lambda_q; \lambda_{(5q)} \rangle = & \\ & D_1(s, \mathbf{k}_\perp) \delta_{\lambda_p \lambda_q} \delta_{\lambda_n \lambda_{(5q)}} + D_2(s, \mathbf{k}_\perp) (\sigma_y)_{\lambda_p \lambda_q} \delta_{\lambda_n \lambda_{(5q)}} + \\ & D_3(s, \mathbf{k}_\perp) \delta_{\lambda_p \lambda_q} (\sigma_y)_{\lambda_n \lambda_{(5q)}} + D_4(s, \mathbf{k}_\perp) (\sigma_x)_{\lambda_p \lambda_q} (\sigma_x)_{\lambda_n \lambda_{(5q)}} + \\ & D_5(s, \mathbf{k}_\perp) (\sigma_y)_{\lambda_p \lambda_q} (\sigma_y)_{\lambda_n \lambda_{(5q)}} + D_6(s, \mathbf{k}_\perp) (\sigma_z)_{\lambda_p \lambda_q} (\sigma_z)_{\lambda_n \lambda_{(5q)}} + \\ & D_7(s, \mathbf{k}_\perp) (\sigma_x)_{\lambda_p \lambda_q} (\sigma_z)_{\lambda_n \lambda_{(5q)}} + D_8(s, \mathbf{k}_\perp) (\sigma_z)_{\lambda_p \lambda_q} (\sigma_x)_{\lambda_n \lambda_{(5q)}} , \end{aligned} \quad (21)$$

where the z - and x -axes are directed along the photon momentum and the momentum transfer \mathbf{k}_\perp , respectively, and the y -axis is orthogonal to the scattering plane.

Now the experimental data on the proton form factor are in agreement with the assumption, that the dominant contribution stems from the amplitude corresponding to the conservation of the s -channel helicities (cf. Ref. [17]). Here we shall use the same assumption and take into account only the amplitude $D_1(s, \mathbf{k}_\perp)$. We thus find

$$\begin{aligned} \langle \lambda_p; \lambda_n | \hat{T}(s, \mathbf{p}_{3\perp}) | \lambda_d; \lambda_\gamma \rangle = & \\ & \frac{i}{8\pi^2 s} \int d^2 \mathbf{k}_\perp \bar{u}_{\lambda_p}(p_3) \hat{\epsilon}_{\lambda_\gamma} \left(\frac{-\hat{k} + m_q}{k^2 - m_q^2} \right) \hat{\epsilon}_{\lambda_d} v_{\lambda_n}(p_4) \\ & \times D^{\gamma d \rightarrow q(5q)}(s, \mathbf{k}_\perp) D_1(s, \mathbf{p}_{3\perp} - \mathbf{k}_\perp). \end{aligned} \quad (22)$$

Furthermore, taking into account that at high energy $p_\gamma \gg \sqrt{s_0}$ and finite momentum transfer $t \simeq |\mathbf{p}_{3\perp}|^2 \simeq s_0$ the momentum k is almost transversal $k = (k_0, \mathbf{k}_\perp, k_z)$, where $k_0 \simeq k_z \simeq O\left(\frac{s_0}{2p_\gamma}\right)$ and $\int d^2 \mathbf{k}_\perp \mathbf{k}_\perp(\dots) \sim \mathbf{p}_{3\perp}$, we find the following representation for the spin structure of the $\gamma d \rightarrow pn$ amplitude:

$$\begin{aligned} \langle \lambda_p; \lambda_n | \hat{T}(s, \mathbf{p}_{3\perp}) | \lambda_d; \lambda_\gamma \rangle = & \\ & \bar{u}_{\lambda_p}(p_3) \hat{\epsilon}_{\lambda_\gamma} (A(s, t) \mathbf{p}_{3\perp} \cdot \boldsymbol{\gamma} + B(s, t) m) \hat{\epsilon}_{\lambda_d} v_{\lambda_n}(p_4) , \end{aligned} \quad (23)$$

where

$$\begin{aligned} A(s, t) = & \frac{i}{8\pi^2 s} \int d^2 \mathbf{k}_\perp \frac{\mathbf{k}_\perp \cdot \mathbf{p}_{3\perp}}{|\mathbf{p}_{3\perp}|^2} \frac{1}{k^2 - m_q^2} \\ & \times D^{\gamma d \rightarrow q(5q)}(s, \mathbf{k}_\perp) D_1^{q(5q) \rightarrow pn}(s, \mathbf{p}_{3\perp} - \mathbf{k}_\perp) , \end{aligned} \quad (24)$$

$$\begin{aligned} B(s, t) = & \frac{i}{8\pi^2 s} \frac{m_q}{m} \int d^2 \mathbf{k}_\perp \frac{1}{k^2 - m_q^2} \\ & \times D^{\gamma d \rightarrow q(5q)}(s, \mathbf{k}_\perp) D_1^{q(5q) \rightarrow pn}(s, \mathbf{p}_{3\perp} - \mathbf{k}_\perp) , \end{aligned} \quad (25)$$

and m is the nucleon mass. In the case of a Gaussian parametrization for $D^{\gamma d \rightarrow q(5q)}(s, \mathbf{k}_\perp)$ and D_1 (in Eqs. (24,25)) the ratio $R = A(s, t)/B(s, t)$ is a smooth function of t . We, furtheron, assume that it is a constant and consider this constant as a free parameter.

The differential cross section for the reaction $\gamma d \rightarrow pn$ then is

$$\begin{aligned} \frac{d\sigma_{\gamma d \rightarrow pn}^I}{dt} &= \frac{1}{64 \pi s} \frac{1}{(p_\gamma^{\text{cm}})^2} \left[S_t |B(s, t)|^2 + S_u |B(s, u)|^2 \right. \\ &\quad \left. + (-1)^{I+1} 2S_{tu} \text{Re}(B(s, t)B(s, u)) \right], \end{aligned} \quad (26)$$

where I is the isospin of the reaction, i.e. $I = 1$ (or 0) for isovector (or isoscalar) photons. The kinematical functions S_t, S_u, S_{tu} in (26) are given by

$$\begin{aligned} S_t &= \frac{1}{6} \sum_{\lambda_\gamma, \lambda_d} \text{Sp} \left[\hat{\epsilon}_{\lambda_\gamma} (R \mathbf{p}_{3\perp} \cdot \boldsymbol{\gamma} + m) \hat{\epsilon}_{\lambda_d} (\hat{p}_4 - m) \right. \\ &\quad \left. \times \hat{\epsilon}_{\lambda_d}^* (R \mathbf{p}_{3\perp} \cdot \boldsymbol{\gamma} + m) \hat{\epsilon}_{\lambda_\gamma}^* (\hat{p}_3 + m) \right], \\ S_u &= \frac{1}{6} \sum_{\lambda_\gamma, \lambda_d} \text{Sp} \left[\hat{\epsilon}_{\lambda_d} (R \mathbf{p}_{3\perp} \cdot \boldsymbol{\gamma} + m) \hat{\epsilon}_{\lambda_\gamma} (\hat{p}_4 - m) \right. \\ &\quad \left. \times \hat{\epsilon}_{\lambda_\gamma}^* (R \mathbf{p}_{3\perp} \cdot \boldsymbol{\gamma} + m) \hat{\epsilon}_{\lambda_d}^* (\hat{p}_3 + m) \right], \\ S_{tu} &= \frac{1}{6} \sum_{\lambda_\gamma, \lambda_d} \text{Sp} \left[\hat{\epsilon}_{\lambda_\gamma} (R \mathbf{p}_{3\perp} \cdot \boldsymbol{\gamma} + m) \hat{\epsilon}_{\lambda_d} (\hat{p}_4 - m) \right. \\ &\quad \left. \times \hat{\epsilon}_{\lambda_\gamma}^* (R \mathbf{p}_{3\perp} \cdot \boldsymbol{\gamma} + m) \hat{\epsilon}_{\lambda_d}^* (\hat{p}_3 + m) \right]. \end{aligned} \quad (27)$$

In order to fix the energy dependence of the amplitude $B(s, t)$ we require that

$$\left. \frac{d\sigma}{dt} \right|_{\theta_{c.m.}=0} \sim \left(\frac{s}{s_0} \right)^{2\alpha_N(0)-2}. \quad (28)$$

Taking into account that $S_t \sim s$ for $s \gg s_0$ we find that

$$B(s, t) \sim \left(\frac{s}{s_0} \right)^{\alpha_N(0)-1/2}. \quad (29)$$

Moreover, a good approximation for the energy dependence of $S_t(\theta_{c.m.} = 0)$ in the region $p_\gamma = 1 \div 7.5$ GeV is

$$S_t|_{\theta_{c.m.}=0} \approx C p_\gamma^2 \quad (30)$$

with $C = (36 \pm 3)$ GeV². Using this approximation we can relate $B(s, t)$ to the Regge-pole exchange amplitude as

$$|B(s, t)|^2 = \frac{1}{C p_\gamma^2} |\mathcal{M}_{\text{Regge}}(s, t)|^2, \quad (31)$$

where

$$\mathcal{M}_{\text{Regge}}(s, t) = F(t) \left(\frac{s}{s_0} \right)^{\alpha_N(t)} \exp \left[-i \frac{\pi}{2} \left(\alpha_N(t) - \frac{1}{2} \right) \right]. \quad (32)$$

Here $\alpha_N(t)$ is the trajectory of the nucleon Regge pole and $s_0 = 4 \text{ GeV}^2 \simeq m_d^2$.

3.3 Nonlinear nucleon Regge trajectories

According to the data on πN backward scattering (see e.g. the review [18]) the nucleon Regge trajectory has a nonlinearity:

$$\alpha_N(t) = \alpha_N(0) + \alpha'_N(0)t + \frac{1}{2}\alpha''_N(0)t^2 K(t), \quad (33)$$

where $\alpha_N(0) = -0.5$, $\alpha'_N(0) = 0.9 \text{ GeV}^{-2}$ are the intercept and slope of the Regge trajectory, $\alpha''_N(0) = 0.20 \div 0.25 \text{ GeV}^{-4}$ is the coefficient of the nonlinear term. In (33) we introduced also a cut-off function $K(t)$. In Ref. [18] it was assumed that $K(t) = 1$. However, in this case the amplitude will grow very fast with s at large t which would violate unitarity. To prevent this fast growth it was taken in Ref. [5] as a powerlike cut-off $K(t) = (1 + t^4/\Lambda^4)^{-1}$. Here we choose the exponential form

$$K(t) = \exp(-\beta t^2) \quad (34)$$

with $\beta = 0.008 \text{ GeV}^{-4}$. We mention that the small value of β does not destroy the parameterization of $\alpha(t)$ for $-t \leq 1.6 \text{ GeV}^2$ found in Ref. [18]. Note also that the phenomenological Regge trajectory (33) with a powerlike or exponential cut-off is nonlinear only for moderate values of t ; at large t the quadratic term becomes small and the trajectory becomes essentially linear again.

On the other hand, the QCD motivated Regge trajectories as suggested by Brisudová, Burakovsky and Goldman (BBG) [21] show a different behaviour at large t . As shown in Ref. [21] the screened quark-antiquark potential

$$V(R) = \left[-\frac{\alpha}{R} + \sigma R \right] \frac{1 - \exp(-\mu R)}{\mu R} \quad (35)$$

with $\sigma = (400 \text{ MeV})^2$, $\mu^{-1} = 0.90 \pm 0.20 \text{ fm}$, $\alpha = 0.21 \pm 0.1$, found in Ref. [24] to describe the lattice QCD data with dynamical Kogut-Susskind fermions, leads to nonlinear meson Regge trajectories. These trajectories can be parametrized on the whole physical sheet as

$$\alpha(t) = \alpha(0) + \gamma [T^\nu - (T - t)^\nu] \quad (36)$$

with $0 \leq \nu \leq 1/2$. The limiting cases $\nu = 1/2$ and $\nu \rightarrow 0$ ($\gamma\nu = \text{const}$) correspond to the square-root trajectory

$$\alpha(t) = \alpha(0) + \gamma [\sqrt{T} - \sqrt{T - t}], \quad (37)$$

and the logarithmic trajectory

$$\alpha(t) = \alpha(0) - (\gamma\nu) \ln \left(1 - \frac{t}{T} \right) \quad (38)$$

respectively. Such trajectories arise not only for heavy quarkonia, but also for light-flavour hadrons.

To find the possible form of nonlinear Regge trajectories for mesons composed of light quarks, Brisudová, Burakovsky and Goldman [21] have considered an analytical model for a string with massless ends and variable string tension. This model describes a colour flux tube stretched between quark and antiquark at the tube ends. The varying string tension was introduced to simulate dynamical effects such as the weakening of the flux tube due to pair ($q\bar{q}$) creation. Within this model they were able to recover the form of the underlying potential for a given Regge trajectory. They found potentials leading to “square-root” and “logarithmic” Regge trajectories and demonstrated, that these potentials are very similar to the screened potential of the unquenched lattice QCD calculations. Moreover, they were able to describe very well all the available meson spectra using a square-root Regge trajectory. Nevertheless, the “logarithmic” form of Regge trajectories can not be excluded by now and new data on higher excited states are necessary.

We know from experiment that the slopes of meson and baryon Regge trajectories are almost the same $\alpha'_N \simeq \alpha'_\rho \simeq 0.9 - 1 \text{ GeV}^{-2}$ (see e.g. the review [9]). The slope is determined by the string tension which depends on the colour charges at the string ends. Therefore, the baryon Regge trajectory can be described by the colour flux model with quark and diquark at the ends (cf Ref. [25]). This means that for the baryon Regge trajectories we can also use the forms suggested by BBG.

When using the QCD motivated trajectories (37) and (38) we take their intercepts and slopes the same as in case of the phenomenological trajectories. Therefore, only a single free parameter will be left. We choose $T = T_B$ as this free parameter and fix it by comparing our results to experimental data.

4 Cross sections for deuteron photodisintegration in the QGSM

4.1 Choice of parameters

The dependence of the residue $F(t)$ on t can be taken from Refs. [15, 16] in the form

$$F(t) = B \left[\frac{1}{m^2 - t} \exp(R_1^2 t) + C \exp(R_2^2 t) \right], \quad (39)$$

where the first term in the square brackets contains the nucleon pole and the second term accounts for the contribution of non-nucleonic degrees of freedom in the deuteron. We adopted the following sets of parameters:

i) for the case of the phenomenological nonlinear trajectory

$$\begin{aligned} \text{Set K: } & B = 3.32 \cdot 10^{-4} \text{ kb}^{1/2} \cdot \text{GeV}, \quad C = 0.7 \text{ GeV}^{-2}, \\ & R_1^2 = 1 \text{ GeV}^{-2}, \quad R_2^2 = -0.1 \text{ GeV}^{-2}, \quad \alpha''_{N(0)} = 0.20 \text{ GeV}^{-4}, \\ \text{Set G: } & B = 4.01 \cdot 10^{-4} \text{ kb}^{1/2} \cdot \text{GeV}, \quad C = 0.7 \text{ GeV}^{-2}, \\ & R_1^2 = 2 \text{ GeV}^{-2}, \quad R_2^2 = 0.03 \text{ GeV}^{-2}, \quad \alpha''_{N(0)} = 0.25 \text{ GeV}^{-4} \end{aligned} \quad (40)$$

and the ratio $R = A(s, t)/B(s, t) = 1$ for both sets K and G. The parameters of the residue (39) in Set K, except the overall normalization factor B and R_1^2 , are the same as in Ref. [15] which were fitted to data on the reaction $pp \rightarrow \pi^+d$ for $-t \leq 1.6 \text{ GeV}^2$. Therefore, in this case we have only two free parameters of the residue B and R_1^2 which we fixed by the experimental data on deuteron photodisintegration at $\Theta_{\text{c.m.}} = 36^\circ$. We note that Set G corresponds to positive values of R_2^2 ;

ii) for the case of the QCD motivated Regge trajectories we have used the parameters of the residue from Set G except an overall normalization factor B taken as $B = 1.8 \cdot 10^{-4} \text{ kb}^{1/2} \cdot \text{GeV}$ for the logarithmic and $B = 2.0 \cdot 10^{-4} \text{ kb}^{1/2} \cdot \text{GeV}$ for the square-root trajectory. Furthermore, we choose $R = A(s, t)/B(s, t) = 2$ for both trajectories (logarithmic and square-root). In order to achieve a good agreement with the data at $\Theta_{\text{c.m.}} = 36^\circ$ the nonlinearity parameter $T = T_B$ was chosen in the interval 1.5-1.7 GeV^2 .

4.2 Energy dependence of the differential cross section

In Fig. 3 we present the energy dependence of $d\sigma/dt \cdot s^{11}$ at different c.m. angles calculated for the case of the phenomenological nonlinear trajectory (33). The experimental points are taken from [1]. The bold solid and dash-dotted lines present results of calculations within the QGSM for parameters of the Set G and Set K, respectively. The thin lines show the results obtained in the case of the linear Regge trajectories with residue parameters from Set G (thin solid line) and Set K (thin dash-dotted line). For $\Theta_{\text{c.m.}} = 36^\circ$ (see the top-left part) all the curves except the thin solid line are in a reasonable agreement with the data. Therefore, for this angle it is also possible to describe the data using a linear nucleon Regge trajectory. However, at large angles $\Theta_{\text{c.m.}} = 52^\circ, 69^\circ$ and 89° the nonlinearity becomes essential since the thin curves underestimate the experimental points substantially. The use of the nonlinear Regge trajectory instead provides a reasonable description of the existing data and reproduces the scaling behavior of $d\sigma/dt \cdot s^{11}$ for $\Theta_{\text{c.m.}} = 69^\circ$ and 89° at energies $E_\gamma \leq 5 \text{ GeV}$. At higher energies all curves drop very fast.

In Fig. 4 the energy dependence of $d\sigma/dt \cdot s^{11}$ at different c.m. angles is calculated for the cases of the square-root (37) (dash-dotted lines) and logarithmic (38) (dashed lines) Regge trajectories. The lower and upper curves were calculated with $T_B = 1.7$ and 1.5 GeV^2 , respectively. As noted before, the ratio of the invariant amplitudes $R = A(s, t)/B(s, t)$ is taken as $R = 2$. It is seen that the result of the square-root trajectory leads to a cross section which underestimates the data for $\Theta_{\text{c.m.}} \geq 52^\circ$, while the logarithmic trajectory provides a reasonable description of the data at all angles (with the exception of a single point at $\Theta_{\text{c.m.}} = 89^\circ, E_\gamma = 4 \text{ GeV}$). Therefore, new measurements of $d\sigma/dt$ at $E_\gamma \geq 5 \text{ GeV}$ will provide a crucial check of the QGSM predictions.

4.3 Angular dependence of the cross section

In Fig. 5 we show the angular dependence of the differential cross section as a function of $\Theta_{\text{c.m.}}$ calculated for $E_\gamma = 1.6 \text{ GeV}$ and 3.98 GeV using the phenomenological nonlinear trajectory (33) with $\alpha''(0) = 0.25 \text{ GeV}^{-4}$ and residue parameters of the set G. Here

we have assumed isovector photon dominance and therefore obtain a forward-backward symmetric cross sections. Both angular distributions have forward and backward peaks, which are mainly related to the choice $R = A(s, t)/B(s, t)=1$ in this case. The agreement between data and calculations is fairly good.

4.4 Forward-backward asymmetry

In Fig. 6 we present the angular dependence of $d\sigma/dt \cdot s^{11}$ at different energies for the logarithmic (38) Regge trajectory. The lower and upper parts correspond to $E_\gamma = 3.98$ and 1.6 GeV, respectively. The two dashed curves in each figure were calculated assuming isovector photon dominance. In this case we have a forward-backward symmetry of the differential cross section. At 1.6 GeV the angular distribution has a dip at $\Theta_{c.m.} = 0^\circ$ and 180° which is related to the different choice of the ratio R ($R = 2$) as compared to the previous case ($R = 1$).

A forward-backward asymmetry arises when we take into account the interference of two amplitudes which describe the contribution of isovector (ρ like) and isoscalar (ω like) photons. In this case the differential cross section can be written as

$$\begin{aligned} \frac{d\sigma_{\gamma d \rightarrow pn}^{\rho+\omega}}{dt} &= \frac{1}{64\pi s} \frac{1}{(p_\gamma^{cm})^2} \left[S_t |B^\rho(s, t) + B^\omega(s, t)|^2 + \right. \\ & S_u |B^\rho(s, u) - B^\omega(s, u)|^2 \\ & \left. + 2S_{tu} \operatorname{Re}(B^\rho(s, t) + B^\omega(s, t))^* (B^\rho(s, u) - B^\omega(s, u)) \right]. \end{aligned} \quad (41)$$

Using the vector dominance model we take

$$B^\omega(s, t) = B^\rho(s, t)/\sqrt{8}, \quad B^\omega(s, u) = B^\rho(s, u)/\sqrt{8}. \quad (42)$$

The data at 1.6 GeV provide an evidence for a forward-backward asymmetry because the values of the differential cross sections at backward angles are smaller than for the corresponding angles in the forward region. The predictions of the simple VDM model with $\rho - \omega$ interference are in qualitative agreement with the data (long-dashed curves). However, for definite conclusions we will need more systematic data at smaller angles in the forward and also in the backward regions.

5 Conclusions

In this work we have analyzed deuteron photodisintegration at GeV energies within the framework of the Quark-Gluon Strings Model with nonlinear Regge trajectories. We have taken into account spin effects assuming the dominance of those amplitudes that conserve s -channel helicities. We have found that the QGSM provides a reasonable description of the new TJNAF data on deuteron photodisintegration at large momentum transfer t and that the energy dependence of $d\sigma/dt$ at $\Theta_{c.m.} = 36 \div 90^\circ$ provides new evidence for a nonlinearity of the Regge trajectory $\alpha_N(t)$. The best agreement with the data can be

achieved using the QCD motivated logarithmic form of the Regge trajectory. However, new data at larger energies will be important to further check the energy behaviour of $d\sigma/dt$ at fixed c.m. angles as predicted by the QGSM.

We have also investigated the angular dependence of the cross section at different energies. The differential cross section may have a dip at forward angles if the amplitude with a charge-like photon coupling ($A(s, t)$) is dominant. By introducing the interference of isovector and isoscalar photon contributions we have calculated the forward-backward asymmetry of the cross section, which can be quite pronounced at $E_\gamma = 1.6$ GeV, but will be a decreasing function of energy. New data for small and large angles (forward and backward) will be important to check these predictions.

References

- [1] E89-012 Collaboration: C. Bochna, B.P. Terburg *et al.*, *Phys. Rev. Lett.* **81** (1998) 4576.
- [2] J. Napolitano *et al.*, *Phys. Rev. Lett.* **61** (1988) 2530; S.J. Freedman *et al.*, *Phys. Rev. C* **48** (1993) 1864.
- [3] J.E. Belz *et al.*, *Phys. Rev. Lett.* **74** (1995) 646.
- [4] S.J. Brodsky and G.R. Farrar, *Phys. Rev. Lett.* **31** (1973) 1153;
V. Matveev, R.M. Muradyan, A.N. Tavkhelidze, *Lett. Nuovo Cimento* **7** (1973) 719
- [5] L.A. Kondratyuk, E. De Sanctis, P. Rossi *et al.*, *Phys. Rev. C* **48** (1993) 2491.
- [6] A.B. Kaidalov, *Z. Phys. C* **12** (1982) 63.
- [7] G. 't Hooft, *Nucl. Phys. B* **72** (1974) 461.
- [8] G. Veneziano, *Phys. Lett. B* **52** (1974) 220; *Nucl. Phys. B* **117** (1976) 519.
- [9] A.B. Kaidalov, in "Surveys in High Energy Physics" **13** (1999) 265.
- [10] A. Casher, J. Kogut and L. Susskind, *Phys. Rev. D* **10** (1974) 732.
- [11] X. Artru and G. Mennesier, *Nucl. Phys. B* **70** (1974) 93.
- [12] A. Casher, H. Neuberger and S. Nussinov, *Phys. Rev. D* **20** (1979) 179.
- [13] B. Andersson, G. Gustafson and C. Peterson, *Phys. Lett. B* **71** (1977) 337; *Z. Phys. C* **1** (1979) 105.
- [14] E. G. Gurvich, *Phys. Lett. B* **87** (1979) 386.
- [15] A.B. Kaidalov, *Sov. J. Nucl. Phys.* **53** (1991) 872.

- [16] C. Guaraldo, A.B. Kaidalov, L.A. Kondratyuk and Ye.S. Golubeva, *Yad. Fiz.* **59** (1996) 1896; *Phys. Atom. Nucl.* **59** (1996) 1832.
- [17] A.B. Kaidalov, L.A.Kondratyuk, D.V. Tchekin, *Yad. Fiz.* **63** (2000) 1474; *Phys. Atom. Nucl.* **63** (2000) 1395.
- [18] V.A. Lyubimov, *Sov. Phys. Uspekhi* **20** (1977) 691.
- [19] UA8 Coll. (A.Brandt *et al.*), *Nucl. Phys. B* **514** (1998) 3.
- [20] A.E. Inopin, hep-th/0012248.
- [21] M.M. Brisudová, L.Burakovsky and T. Goldman, *Phys. Rev. D* **61** (2000) 054013.
- [22] A.B. Kaidalov, *JETP Lett.* **32** (1980) 474.
- [23] A.B. Kaidalov, in “QCD at 200 TeV”, edited by L. Cifarelli and Yu. Dokshitzer, Plenum Press, N.Y. and London, 1992, p.1
- [24] K.D. Born et al., *Phys. Rev. D* **40** (1989) 1653.
- [25] I. Kobzarev et al., *Sov. J. Nucl. Phys.* **45** (1987) 330.

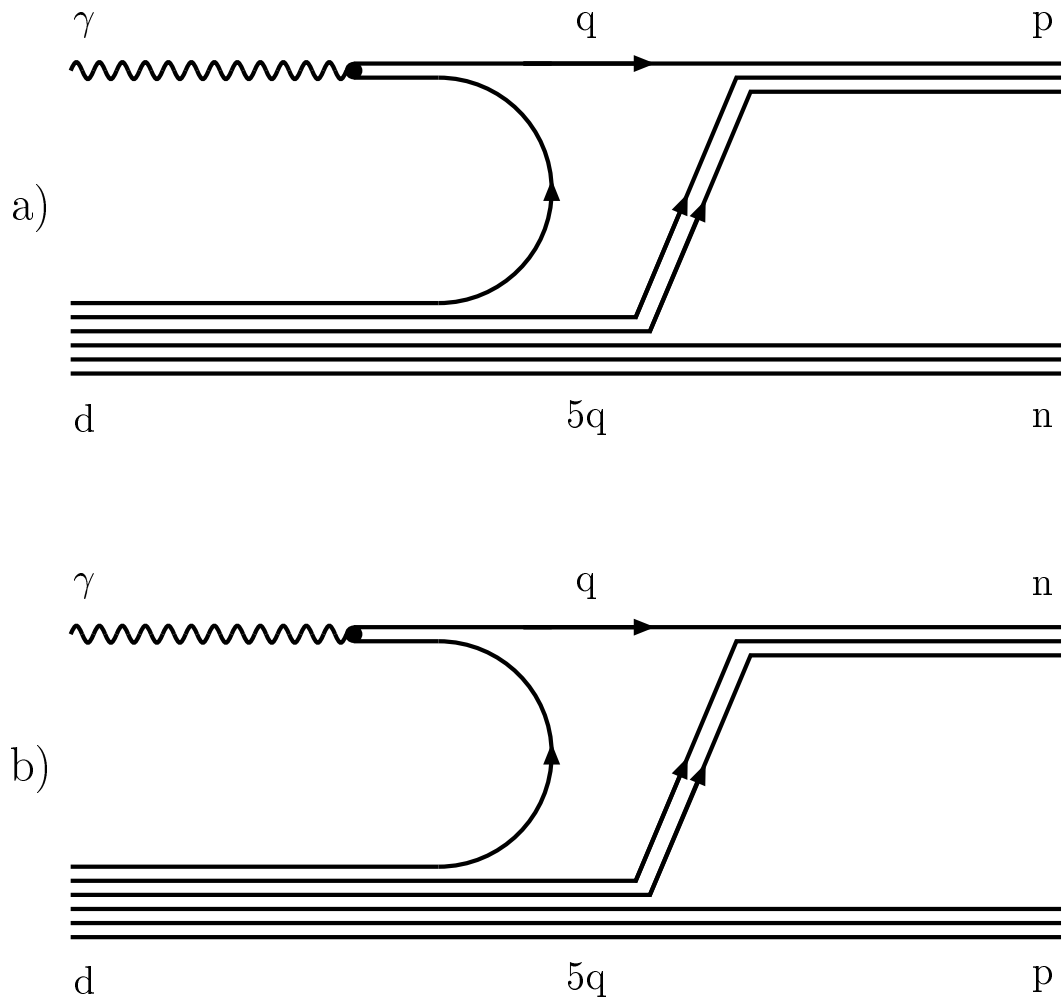


Figure 1: Diagrams describing three valence quark exchanges in t - (a) and u -channels (b).

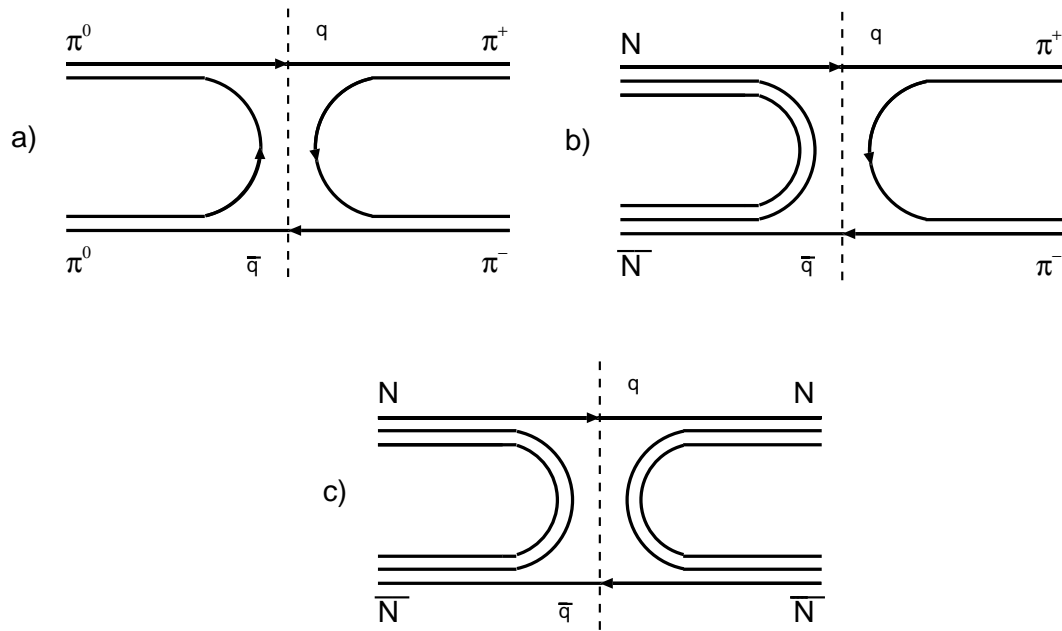


Figure 2: Planar diagrams describing the binary reactions a) $\pi^0\pi^0 \rightarrow \pi^+\pi^-$, b) $N\bar{N} \rightarrow \pi^+\pi^-$, c) $p\bar{p} \rightarrow N\bar{N}$.

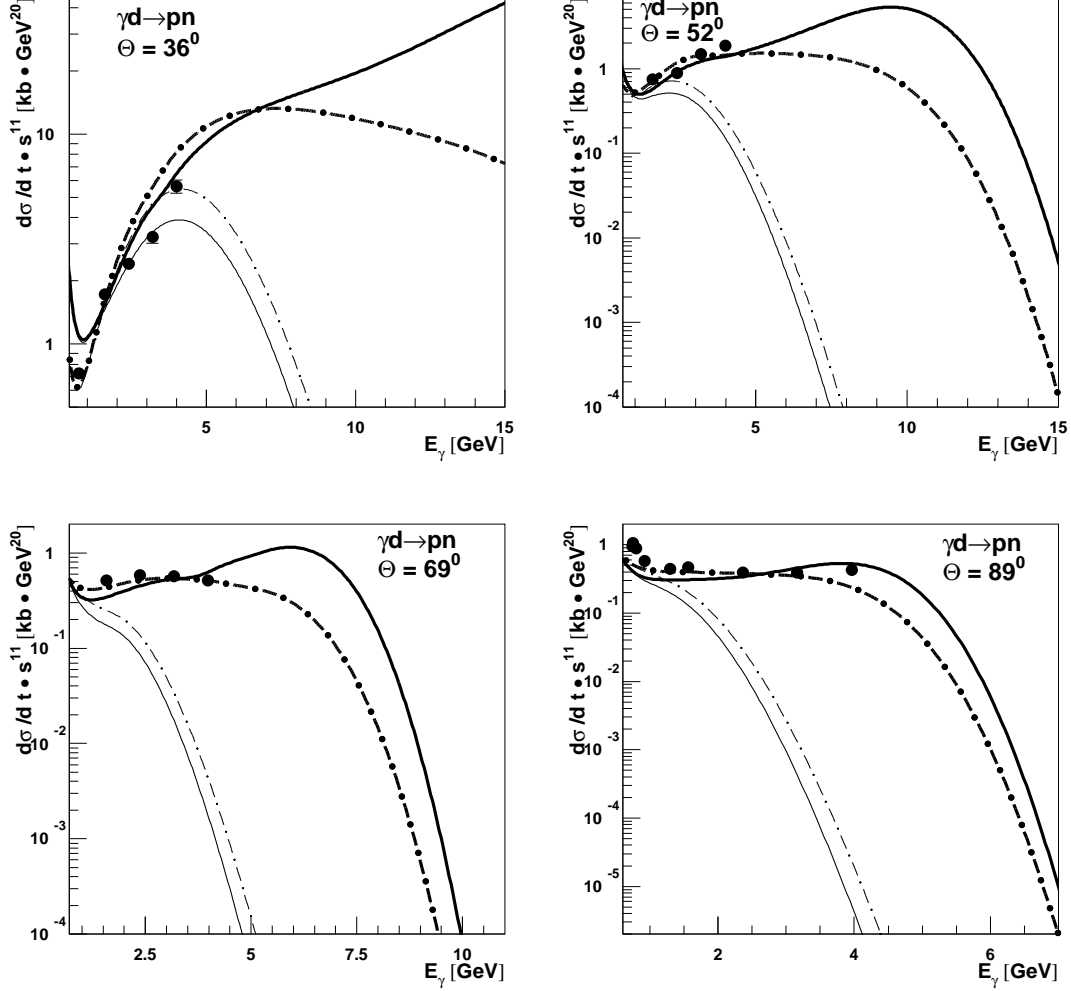


Figure 3: Differential cross section for the reaction $\gamma d \rightarrow pn$ (multiplied by s^{11}) as a function of the photon lab. energy E_γ at different angles in the center-of-mass frame in comparison to the experimental data from Ref. [1]. The bold solid and dash-dotted curves present results of calculations using a phenomenological Regge trajectory for parameter Set G and Set K, respectively. The thin lines show the results obtained in the case of the linear Regge trajectories, i.e. for $\alpha''_{N(0)} = 0$, with the same parameters of the residue as in Set G (solid line) and Set K (dash-dotted line).

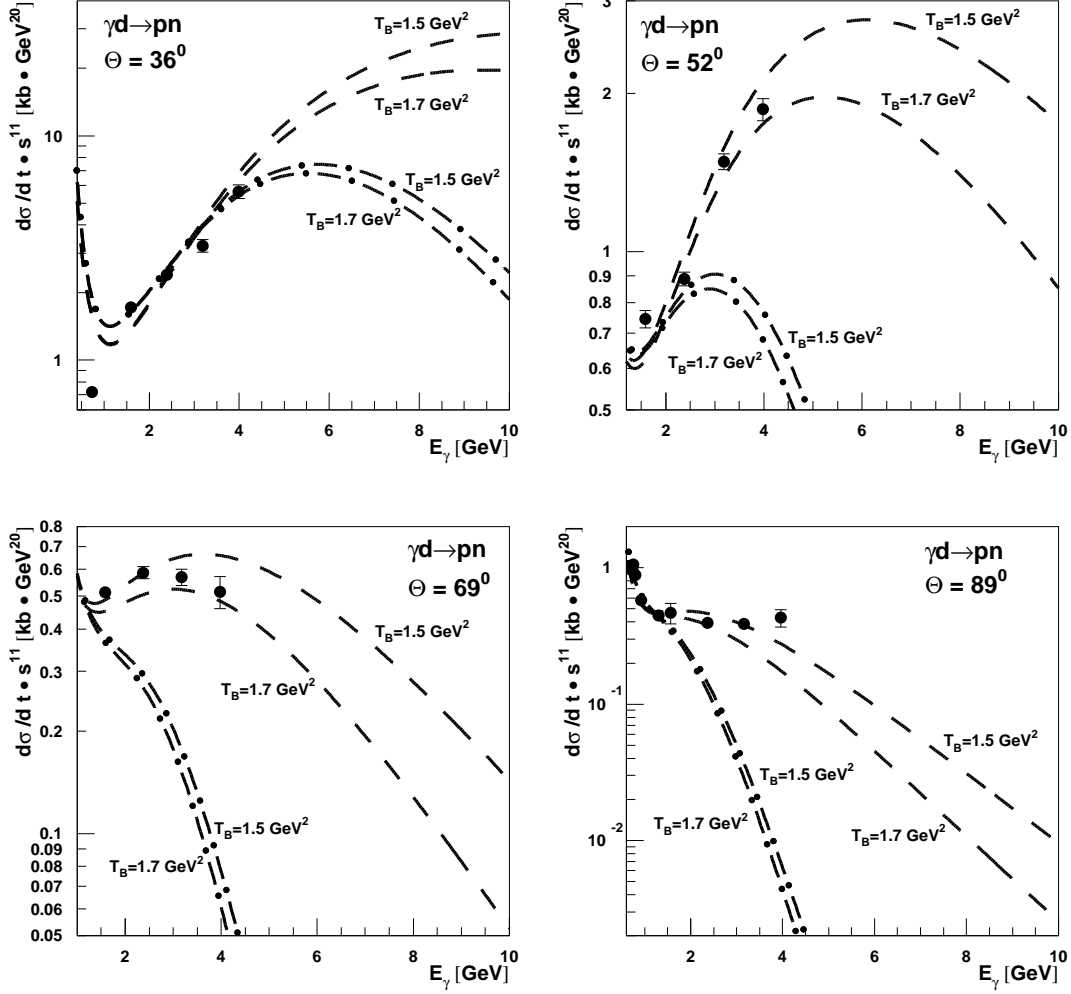


Figure 4: Differential cross section for the reaction $\gamma d \rightarrow pn$ (multiplied by s^{11}) as a function of the photon lab. energy E_γ at different angles in the center-of-mass frame in comparison to the experimental data from Ref. [1]. The dashed and dash-dotted curves are calculated using the logarithmic and square-root Regge trajectories, respectively.

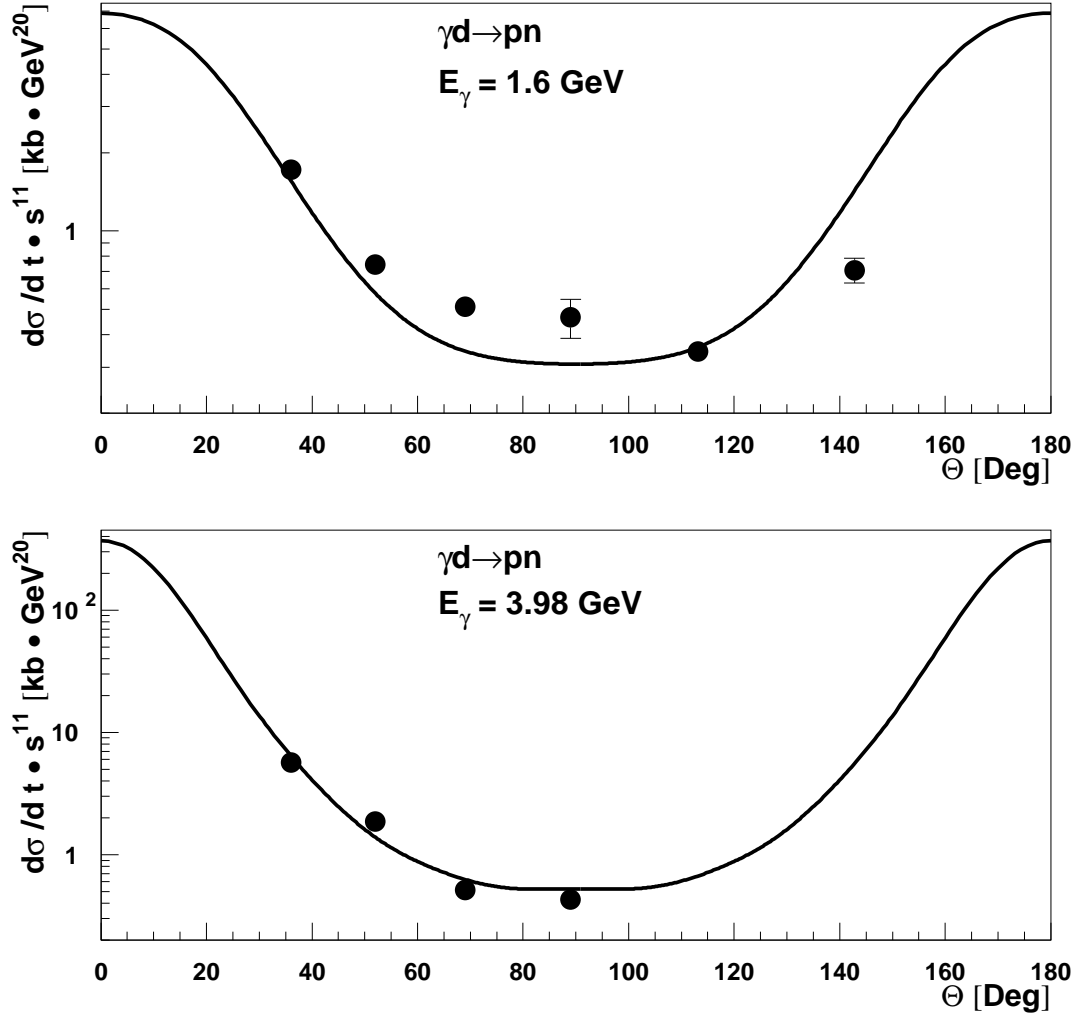


Figure 5: Differential cross section for the reaction $\gamma d \rightarrow pn$ (multiplied by s^{11}) as a function of the c. m. angle for $E_\gamma = 1.6 \text{ GeV}$ and 3.98 GeV (upper and lower parts, respectively). The experimental data are from Ref. [1]. The bold solid curves are results of calculations using the phenomenological Regge trajectory for parameter Set G.

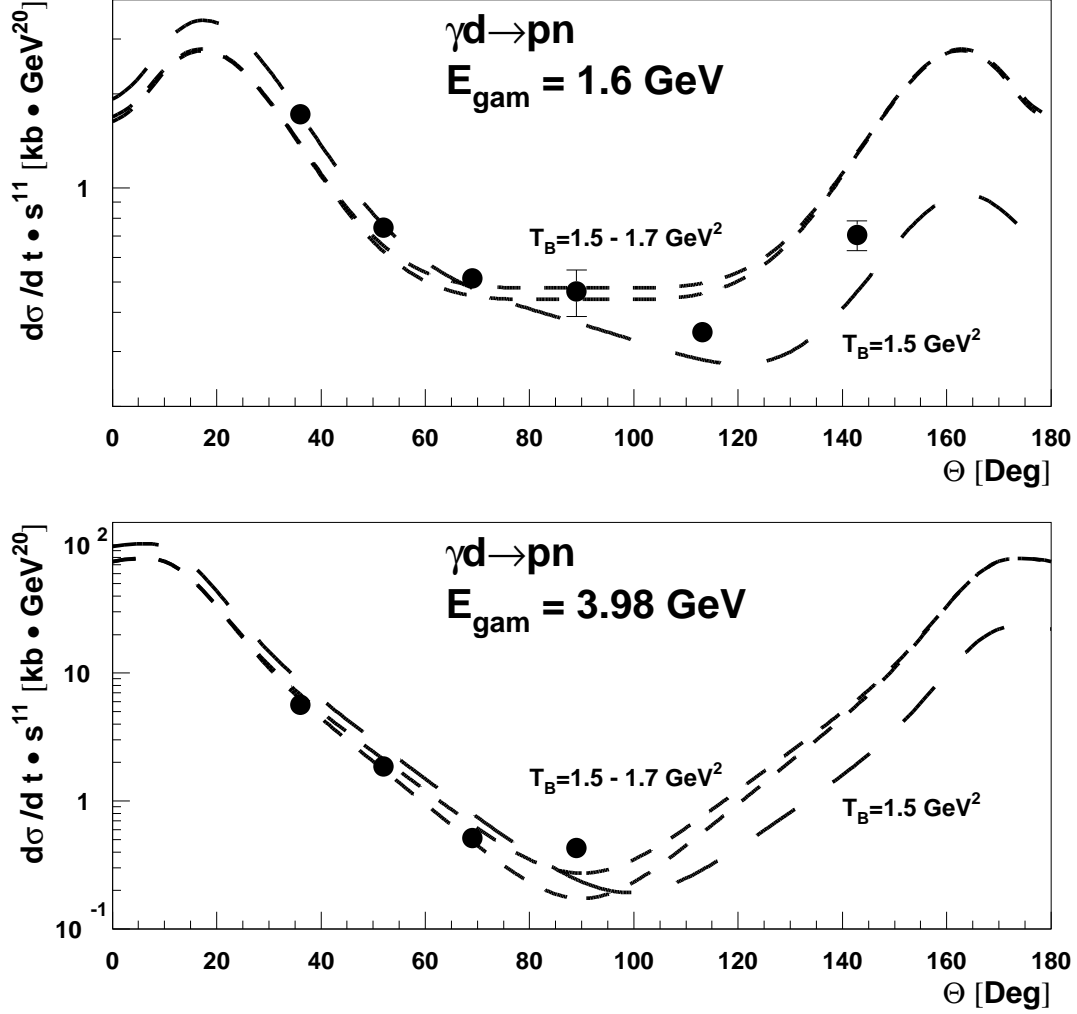


Figure 6: Differential cross section for the reaction $\gamma d \rightarrow pn$ (multiplied by s^{11}) as a function of the c. m. angle for $E_\gamma = 1.6 \text{ GeV}$ and 3.98 GeV (upper and lower parts, respectively). The experimental data are from Ref. [1]. The dashed curves are calculated using logarithmic Regge trajectories with $T_B = 1.5$ and 1.7 GeV^2 . The long-dashed curve presents the result of calculations which take into account the interference of the isoscalar and isovector parts of the $\gamma d \rightarrow pn$ amplitude (see text).